



HAL
open science

Entropy models for the description of the solid–liquid regime of deep eutectic solutions

Laura J.B.M. Kollau, Mark Vis, Adriaan van den Bruinhorst, Remco Tuinier, Gijsbertus de With

► **To cite this version:**

Laura J.B.M. Kollau, Mark Vis, Adriaan van den Bruinhorst, Remco Tuinier, Gijsbertus de With. Entropy models for the description of the solid–liquid regime of deep eutectic solutions. *Journal of Molecular Liquids*, 2020, 302, pp.112155 -. 10.1016/j.molliq.2019.112155 . hal-03489683

HAL Id: hal-03489683

<https://hal.science/hal-03489683>

Submitted on 22 Aug 2022

HAL is a multi-disciplinary open access archive for the deposit and dissemination of scientific research documents, whether they are published or not. The documents may come from teaching and research institutions in France or abroad, or from public or private research centers.

L'archive ouverte pluridisciplinaire **HAL**, est destinée au dépôt et à la diffusion de documents scientifiques de niveau recherche, publiés ou non, émanant des établissements d'enseignement et de recherche français ou étrangers, des laboratoires publics ou privés.



Distributed under a Creative Commons Attribution - NonCommercial 4.0 International License

Entropy models for the description of the solid–liquid regime of deep eutectic solutions

Laura J.B.M. Kollau^{a,b,c}, Mark Vis^{a,b,c}, Adriaan van den Bruinhorst^{a,b,c},
Remco Tuinier^{a,b,d}, Gijsbertus de With^a

^a*Laboratory of Physical Chemistry, Department of Chemical Engineering and Chemistry, Eindhoven University of Technology, The Netherlands*

^b*Institute for Complex Molecular Systems, Eindhoven University of Technology, The Netherlands*

^c*Laboratoire de Chimie, Ecole Normale Supérieure de Lyon, France*

^d*Van 't Hoff Laboratory for Physical and Colloid Chemistry, Debye Institute for Nanomaterials Science Utrecht University, The Netherlands*

Abstract

A necessary prerequisite for applying deep eutectic solutions (DESs) is to understand the phase behavior and to be able to quantify the liquid window of these mixtures. The non-ideality of the phase behavior is determined by the contributions of excess entropy and enthalpy. While the total Gibbs energy of mixing can be inferred from the solid–liquid phase behavior, the entropic and enthalpic contributions can not be distinguished. Hence, by assuming ideal mixing entropy, all excess free energy is captured as an enthalpic contribution. The ideal mixing entropy provides a reasonable description when the components are similar in size and shape. This is not always the case for the components typically used in DESs. Here, the suitability of two non-ideal entropy models is investigated, aiming to describe the phase behavior of DESs more accurately. First, by using Flory–Huggins entropy accounting for the different molar volumes of the components, we show that ideal entropy of mixing underestimates the entropic contribution for mixtures of components often used for DESs. The value of molar volume employed has a significant influence on the resulting entropy of mixing and thus on the resulting enthalpy. Second, correcting for the molar area as well, using the Staverman–Guggenheim entropy, appears to have negligible impact for the

Email address: m.vis@tue.nl (Mark Vis)

Preprint submitted to Journal of Molecular Liquids

November 8, 2019

compounds considered. Both the use of a non-ideal mixing entropy and the specific choice of the molar volume significantly affect the obtained enthalpy of mixing and will thus alter the interaction parameters, obtained using a Redlich–Kister-like mixing enthalpy, as compared to models based on ideal mixing entropy.

Keywords: Deep eutectic solvents, thermodynamics, phase diagrams, entropy, melting point depression

1. Introduction

In 1884 Frederick Guthrie [1] coined the term eutectic by combining the Greek words ‘ευ’—meaning good/easy—with ‘τρχειν’—which means melting—and defined it as:

“(…) bodies made up of two or more constituents, which constituents are in such proportion to one another as to give the resultant compound body a minimum temperature of liquefactions—that is, a lower temperature of liquefaction than that given by any other proportion.”

Following this, Guthrie connected solubility to melting [2]:

“The phenomenon of fusion per se is continuous with, and nothing more than an extreme case of, liquefaction by solution. (...) Hence the question, is this a case of fusion or solution is to be answered by the reply, it is continuous with both.”

At the beginning of this century the term ‘deep eutectic solvents’ was first used [3] for a mixture of two components showing eutexia in an extreme form: a remarkably large melting point depression. This results for instance in a liquid binary mixture made from components, which are by themselves solid at room temperature. It was shown that this feature could be extended to other mixtures of similar constituents resulting in mixtures with tuneable physical properties. With this, the potential of these mixtures as designer solvents was founded, considering that their properties can be tailored based on the nature of its constituents. Hence, it is not a surprise that since the term DES was introduced, numerous studies on the properties of these mixtures were performed, postulating applications for solvents like biomass processing [4–7], CO₂ capture[8, 9] and many others [10–12]. It should be

27 noted that even though DESs are often treated as a new class of solvents [13],
 28 eutectic mixtures were applied widely already as pharmaceuticals in order to
 29 solubilize or liquefy specific compounds [14–18], as phase change material
 30 [19–26], and in liquid crystals [27–30].

31 *1.1. The solubility limits of non-ideal eutectic mixtures*

32 Phase diagrams describe the phase behavior and are essential when de-
 33 signing industrial products and processes. Understanding the phase behavior
 34 is needed to be able to quantify the solid–liquid coexistence as a function of
 35 composition, which provides the melting point depression, and to shed light
 36 on the liquid window of these mixtures. However, little work is yet directed
 37 towards phase diagrams and/or the relation between the melting point de-
 38 pressions of eutectic mixtures with large melting point depressions and the
 39 properties of its constituents.

40 The aim here is to describe the molar Gibbs energy of mixing g and to
 41 differentiate between the contributions resulting from entropy s and enthalpy
 42 h :

$$43 \quad g = h - Ts \quad (1)$$

44 where g can directly be related to experimentally obtained solid–liquid phase
 45 diagrams as follows. Since g is the molar free energy of mixing, the change
 46 $\Delta\mu_i(x_i)$ in chemical potential due to mixing for component i as a function of
 47 mole fraction x_i follows as:

$$48 \quad \left(\frac{\partial ng}{\partial n_i} \right)_{p,T,n_{j \neq i}} = \Delta\mu_i(x_i) = RT \ln a_i, \quad (2)$$

49 where n_i is the number of moles of component i , $n = \sum_i n_i$, a_i is the activity,
 50 and $\Delta\mu_i(x_i) = \mu_i(x_i) - \mu_i^*$. The change $\Delta\mu_i(x_i)$ in chemical potential is in
 51 turn related to the melting point T of the mixture according to:

$$52 \quad \frac{\Delta\mu_i(x_i)}{RT} = \frac{\Delta H_i}{R} \left(\frac{1}{T_i^*} - \frac{1}{T} \right). \quad (3)$$

53 Here the enthalpy of fusion ΔH_i is assumed to be independent of temperature
 54 and T_i^* is the melting point of the pure component.

55 For ideal mixtures the melting point depression originates from an in-
 56 crease in configurations—i.e., entropy—when mixing components in the liq-
 57 uid state. In this case the enthalpy $h = h^{\text{id}} = 0$ resulting in:

$$58 \quad g = g^{\text{id}} = -Ts^{\text{id}}. \quad (4)$$

59 For s^{id} one generally uses the Gibbs entropy, which results from Boltzmann's
 60 equation comprising the probability of the number of microstates in a mix-
 61 ture, i.e. the number of complexions, yielding:

$$62 \quad \frac{g^{\text{id}}}{RT} = \sum_i x_i \ln x_i. \quad (5)$$

63 which results, via Equation (2), in an expression for $\Delta\mu_i$, which reads:

$$64 \quad \frac{\Delta\mu_i}{RT} = \ln x_i. \quad (6)$$

65 Generally, however, there is a need to account for enthalpic interactions
 66 when describing deep eutectic mixtures. Enthalpic interactions can be in-
 67 cluded using excess functions for the Gibbs energy, g^e , defined by:

$$68 \quad g = g^{\text{id}} + g^e. \quad (7)$$

69 For example, for a binary mixture, regular solution theory [31], where the
 70 enthalpic contributions can be quantified using one interaction parameter χ ,
 71 leads to:

$$72 \quad \frac{h^e}{RT} = \chi x_1 x_2. \quad (8)$$

73 We showed [32] that the description of the phase boundaries can be improved
 74 when eq. (8) is expanded using an orthogonal Redlich–Kister-like polynomial
 75 [33–36]:

$$76 \quad \frac{h^e}{RT} = x_1 x_2 [p_0 + p_1 \mathcal{P}_1(x_1 - x_2) + p_2 \mathcal{P}_2(x_1 - x_2) + \dots], \quad (9)$$

77 where $\mathcal{P}_k(x_1 - x_2)$ is the Legendre polynomial of order k as a function of the
 78 variable $x_1 - x_2$. Terminating the expansion after first order, using $\mathcal{P}_1(x_1 -$
 79 $x_2) = x_1 - x_2$,

$$80 \quad \frac{h^e}{RT} = x_1 x_2 [p_0 + p_1 (x_1 - x_2)] \quad (10)$$

81 was found to yield a description at least as good as a commonly used ther-
 82 modynamic engineering model to describe two-phase equilibria, namely non-
 83 random two-liquid theory (NRTL) [37–40]. The advantage of using the or-
 84 thogonal Redlich–Kister-like polynomial rather than NRTL is that the zeroth

85 order parameter p_0 can be identified still as the χ parameter of regular solu-
 86 tion theory and that its value is unaffected by the addition of the orthogonal
 87 higher order terms. Thus, higher order terms can be added when this is sta-
 88 tistically justified, while not affecting the physical interpretation of regular
 89 solution theory. In this work we employ the first order expansion, eq. (10),
 90 but if the addition of the first order term does not statistically improve the
 91 fit of the phase diagram, we set $p_1 = 0$ [32], thus essentially using eq. (8).

92 As a direct result from using the ideal Gibbs entropy s^{id} all the excess free
 93 energy is captured effectively as an enthalpic contribution. The ideal mixing
 94 entropy s^{id} provides a reasonable description for the number of complexions
 95 when the components are similar in size and shape. This is, of course, far
 96 from the actual situation for the components typically used in DESs. Here
 97 both the volumes as well as the surface areas of the components may differ
 98 to a smaller or larger extent.

99 To get a better understanding of the enthalpic interactions resulting in
 100 the melting point depressions observed, we employ here different entropy
 101 models in order to isolate the enthalpic contributions as much as possible.
 102 We compare the following entropy models for binary mixtures in this work.
 103 First, the mole fraction-based ideal Gibbs entropy s^{id} —now labelled as s^x —
 104 is used as reference, eq. (11a). Second, we use the non-ideal volume fraction-
 105 based entropy model from Flory–Huggins theory, s^ϕ , eq. (11b). As a third,
 106 we employ the Stavermann–Guggenheim correction s^θ , eq. (11c), which also
 107 takes surface area in account:

$$108 \quad s^x = x_1 \ln x_1 + x_2 \ln x_2, \quad (11a)$$

$$109 \quad s^\phi = x_1 \ln \phi_1 + x_2 \ln \phi_2, \quad (11b)$$

$$110 \quad s^\theta = x_1 \ln \phi_1 + x_1 Q_1 \ln \left(\frac{\theta_1}{\phi_1} \right) + x_2 \ln \phi_2 + x_2 Q_2 \ln \left(\frac{\theta_2}{\phi_2} \right). \quad (11c)$$

111 Here ϕ and θ denote the volume fraction and surface fraction, defined by:

$$112 \quad \phi_i(x_i) = \frac{x_i V_{\text{m},i}}{\sum_j x_j V_{\text{m},j}}, \quad (12)$$

$$113 \quad \theta(x_i) = \frac{x_i A_{\text{m},i}}{\sum_j x_j A_{\text{m},j}}, \quad (13)$$

114 where we take $V_{\text{m},i}$ as the van der Waals molecular volume for component
 115 i and $A_{\text{m},i}$ as the van der Waals molecular surface area for component i .

116 Further, Q_i is a direct function of ϕ_i and θ_i [41]:

$$117 \quad Q_i = \frac{1 - \frac{\phi_i}{x_i}}{1 - \frac{\phi_i}{\theta_i}}. \quad (14)$$

118 *1.1.1. Flory–Huggins entropy of mixing*

119 The Flory–Huggins entropy of mixing accounts for unequally sized molecules
120 and results in the following expression for the change in chemical potential
121 upon mixing:

$$122 \quad \frac{\Delta\mu_i}{RT} = \ln \phi_i + \left(1 - \frac{\phi_i}{x_i}\right). \quad (15)$$

123 From this expression it follows that ideal mixing entropy is only achieved in
124 case of equal molar volumes of both components. The molar volumes (based
125 on different methods, see experimental section) as well as the other relevant
126 fusion properties of the components used in this work are listed in Table 1.

127 The effect of a difference in molecular volumes on the liquidus is schemat-
128 ically depicted in Figure 1. In panel I solid–liquid equilibria based on the
129 ideal mixing entropy using identical fusion properties are depicted as dashed
130 curves. This results in a fully symmetrical phase diagram. The phase bound-
131 aries resulting from a mixing entropy when the molar volume of component
132 B is larger than component A are plotted in panel II as the dashed curves.
133 The solid curves demonstrate the influence of a negative mixing enthalpy,
134 eq. (8) with $\chi < 0$, on the phase behavior. Overall, both a difference in
135 molar volumes as well as binary attractions lead to a decrease of the eutectic
136 temperature.

137 *1.1.2. Staverman–Guggenheim entropy of mixing*

138 Guggenheim [42] showed that the Flory–Huggins model overestimates the
139 entropy of mixing, because the connectivity of sites in a molecule reduces the
140 number of possible configurations, and derived a correction term. Staverman
141 [43] essentially derived the same expression and applied it to more compli-
142 cated molecules. The expression for the change in chemical potential upon
143 mixing is:

$$144 \quad \frac{\Delta\mu_i}{RT} = \ln \phi_i - Q_i \ln \left(\frac{\phi_i}{\theta_i}\right). \quad (16)$$

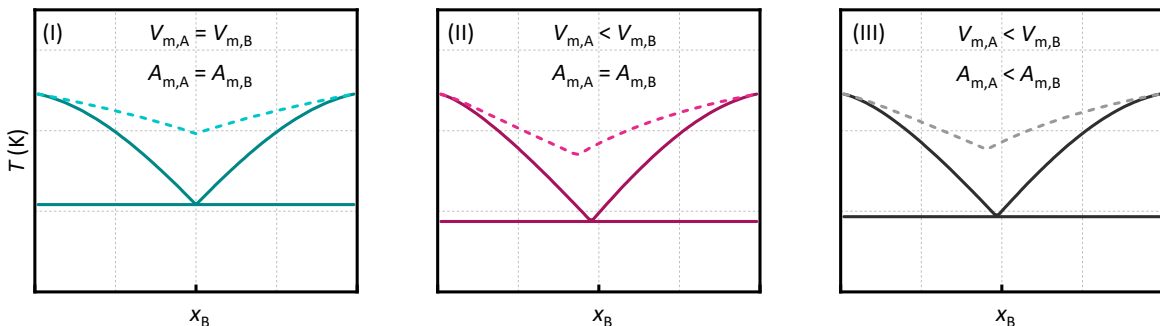


Figure 1: Schematic illustrations of the effect of molecular volume and surface on symmetrical eutectic phase behavior: (I) Symmetric phase diagrams where both components have identical molecular volumes (V_m) and surfaces (A_m). (II) The influence of different molecular volumes; $V_{m,A} : V_{m,B} = 1 : 5$. (III) The influence of different molecular volumes and surface; $A_{m,A} : A_{m,B} = 1 : 10$. Dashed curves: Predictions for athermal mixtures ($\chi = 0$) with mixing entropy only. Solid curves: Predictions for the same mixtures with attraction between the different components.

145 The relevant experimental parameters are listed in Table 1.

146 Panel III in fig. 1 shows a slightly higher eutectic temperature for this
 147 entropy model compared to the Flory–Huggins entropy in panel II. The
 148 Staverman–Guggenheim model contains, besides the molecular and volume
 149 fraction, the surface fraction and requires as additional parameter the num-
 150 ber of nearest neighbors for each compound. Recently Krooshof *et al.* showed
 151 that the number of nearest neighbours is directly related to the molar, vol-
 152 ume, and surface fraction through eq. (14), which enables to further simplify
 153 the expressions [41].

154 1.1.3. Model systems

155 The systems used here to demonstrate the different entropy models are
 156 mixtures of the salt tetrapentylammonium bromide (Pe_4NBr) with erythritol,
 157 succinic acid, and pimelic acid, see Figure 2. The selected binary mixtures
 158 differ in one component and non-ideality. This allows for the evaluation
 159 of the suitability of the described thermodynamic models for DESs with
 160 different effective strengths of interaction. **We have previously published**
 161 **detailed phase diagrams for these mixtures elsewhere and will reuse that**
 162 **information for this work [32].** The earlier obtained interaction parameters,
 163 based on ideal mixing entropy, suggest attractions for the mixtures of Pe_4NBr

164 in the order pimelic acid > succinic acid > erythritol [32].

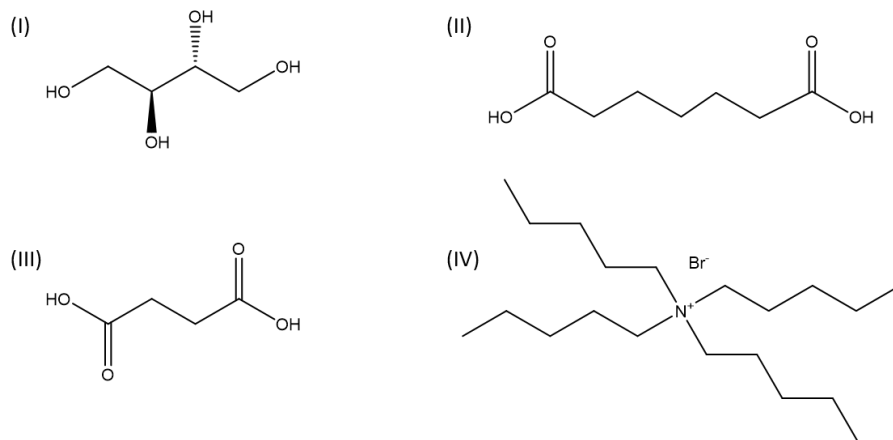


Figure 2: Molecular structures of the various components studied in this work. (I) erythritol, (II) pimelic acid, (III) succinic acid, and (IV) tetrapentylammonium bromide (Pe₄NBr).

Table 1: Melting point T^* , enthalpy of fusion ΔH , molar volume V_m , and molar surface A_m of individual components.

Component	T^* [K]	ΔH [J mol ⁻¹]	V_m [cm ³ mol ⁻¹]			A_m [10 ⁹ cm ² mol ⁻¹]	
	<i>a</i>	<i>a</i>	<i>a</i>	<i>b</i>	<i>c</i>	<i>b</i>	<i>c</i>
Erythritol	394.7	39300.7	83.7	46.4	67.4	11.7	9.9
Succinic acid	460.0	37105.1	75.7	41.9	60.5	10.6	8.8
Pimelic acid	378.5	26074.0	120.0	66.5	90.1	16.5	12.8
Pe ₄ NBr	375.9	40140.5	344.2	190.7	234.8	46.2	33.4

^a Measured experimentally, ^b estimated van der Waals volume/area according to Bondi[44], ^c estimated van der Waals volume/area according to Molecular Modeling Pro software.

165 2. Results and discussion

166 The results for the mixture of erythritol with Pe₄NBr are displayed in
 167 Figure 3 and listed in Table 2. Figure 3 panel I displays the entropy of
 168 mixing s of the mixture versus the composition x . It clearly illustrates the

169 difference between the models for the calculation of s . It shows that the
170 Gibbs entropy of mixing s^x is smaller than the Flory–Huggins estimation for
171 the entropy of mixing s^ϕ . It appears that the differences in available surface
172 between the components, Staverman–Guggenheim entropy of mixing, s^θ , are
173 too small to produce significant differences in entropy, and it is not necessary
174 to take these into account when describing the phase behavior.

175 What is remarkable, though, is that the precise value of the molar volume
176 used has a significant influence on the resulting entropy of mixing. Here
177 we considered molar van der Waals volumes resulting from the Molecular
178 Modeling Pro software s_{MMP}^j , and molar van der Waals volumes from an
179 empirical correlation with molar volumes based on Bondi’s estimates for the
180 van der Waals volume s_{Bondi}^j [44]. The values used for the volumes as well as
181 the surfaces are listed in Table 1. Somewhat surprisingly, as both methods
182 intend to estimate the van der Waals volume, not only the absolute values
183 differ but also the ratios between the components. This causes the entropy
184 to differ, according to the value of the molar volumes used, in such a way
185 that a larger s is obtained when the difference in molar volume between the
186 components of the mixture is larger. For the particular case at hand, this is
187 the estimate resulting from the correlation based on Bondi’s estimates [44].

188 In Figure 3 panel II the effect of the entropy models on the resulting
189 phase diagrams, assuming zero enthalpy of mixing, is demonstrated. It shows
190 that using the Flory–Huggins entropy in combination with molar van der
191 Waals volumes estimated from the correlation mentioned before [44], results
192 in the largest melting point depression without invoking enthalpic interac-
193 tions. However, still a significant difference exists when compared to the
194 measured melting point depressions (symbols). Therefore it can be con-
195 cluded that entropy alone is not enough to explain the observed melting
196 point depressions.

197 When fitting phase diagrams to experimental data through eq. (3), the use
198 of different models for the entropy of mixing result in different values for the
199 enthalpies of mixing h , as pictured in Figure 3 panel III (with the resulting
200 phase diagrams shown in panel IV). It clearly shows that for s^x , where the
201 entropy of mixing is underestimated, the enthalpy of mixing is the highest,
202 as it needs to compensate to obtain approximately the same Gibbs energy
203 to fit the experimentally obtained phase diagram. The difference amounts
204 to about 10%. This difference in enthalpic contributions is also visible in
205 the interaction parameter χ , listed in Table 2. It shows that for s^x , the
206 interaction parameter χ is significantly larger in magnitude, almost differing

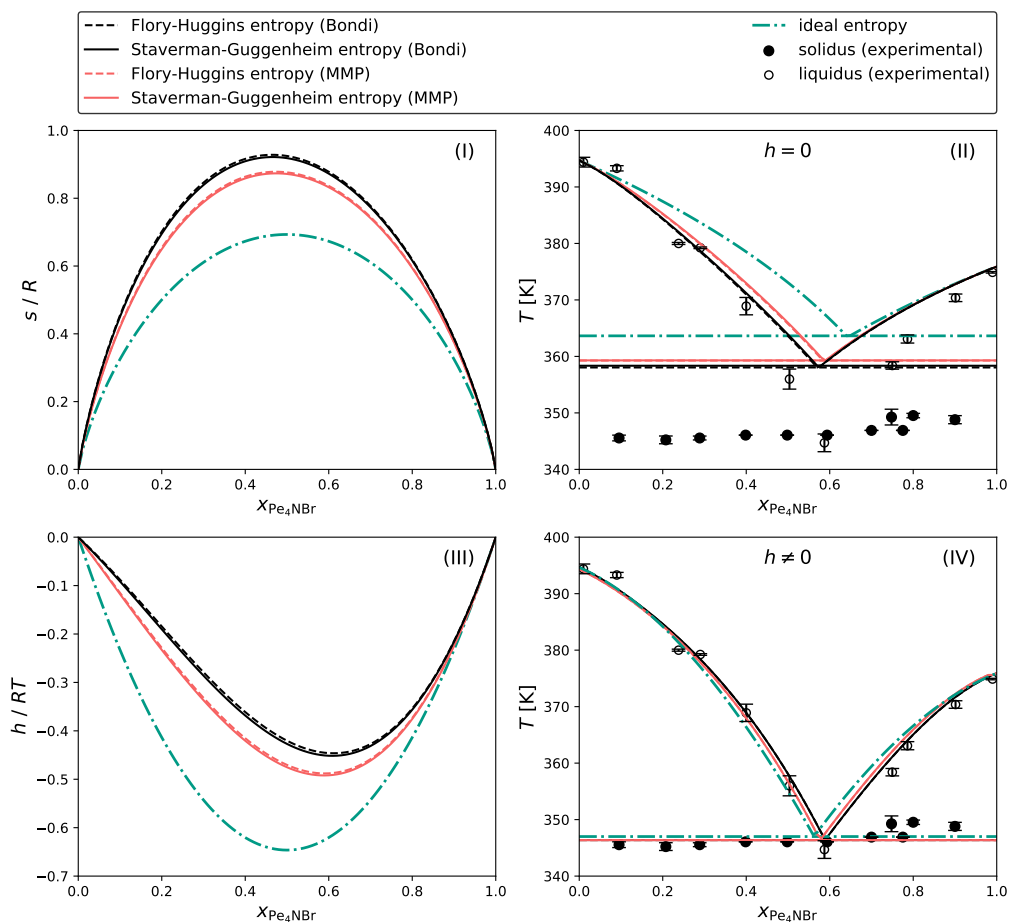


Figure 3: Diagrams for Pe_4NBr –erythritol describing (I) the entropy of mixing, (II) the melting point depression predicted based on entropy alone ($h = 0$, curves) compared to experimental data (symbols), (III) the enthalpy of mixing obtained after fitting measured melting point depressions, and (IV) the fitted melting point depressions compared to experimental data. Various entropy models are used: ideal, Flory–Huggins, and Staverman–Guggenheim. The latter two are combined with van der Waals volumes and areas estimated using the Molecular Modeling Pro software (MMP) and Bondi’s method. Experimental data taken from Ref. 32.

207 by unity, than when s^ϕ is employed. Also the different molar volumes, s_{Bondi}^ϕ
 208 and s_{MMP}^ϕ (based on Bondi and Molecular Modeling Pro, respectively), result
 209 in differences in interaction parameters of about 0.2. As expected, applying
 210 the Staverman–Guggenheim entropy of mixing does not affect the interaction
 211 parameters significantly. The resulting phase diagrams in Figure 3 panel IV
 212 are nearly indistinguishable, which is confirmed by the resulting eutectic
 213 temperatures T_e and eutectic composition x_e also listed in Table 2, which do
 214 not differ significantly.

215 The behavior of the other mixtures, succinic acid or pimelic acid with
 216 Pe_4NBr , given in Table A.1 and shown in Figure A.1 and Figure A.2, is
 217 similar and confirms that accounting for volumes according to Flory–Huggins
 218 is necessary when the components differ in size. This was already pointed
 219 out by Fowler and Guggenheim for $V_{\text{m},1}/V_{\text{m},2} > 2$ [45]. Even though the
 220 magnitude of the mixing enthalpy is affected by the choice of specific entropy
 221 model, the trends in non-ideality observed earlier [32] are preserved.

Table 2: Results of the mixture erythritol with Pe_4NBr . Listed are the theory used for the entropy of mixing s , the interaction parameter χ , p_1 as the second fit parameter [32], the eutectic temperature T_e , the eutectic composition x_e , and the standard error SE between the fit of the phase diagram and the data points.

System	s	χ	p_1	T_e [K]	x_e	SE [K]
Erythritol– Pe_4NBr	s^x	−2.61	0	346.9	0.56	2.5
	s_{Bondi}^ϕ	−1.68	−0.88	346.4	0.59	2.0
	s_{Bondi}^θ	−1.71	−0.87	346.4	0.59	2.0
	s_{MMP}^ϕ	−1.88	−0.75	346.4	0.59	2.0
	s_{MMP}^θ	−1.90	−0.74	346.4	0.59	2.0

222 3. Conclusions

223 We have shown that an ideal entropy of mixing underestimates the entropic
 224 contribution for mixtures of components often used for DESs. Ac-
 225 counting for volumes of the components according to Flory–Huggins the-
 226 ory is necessary when the components significantly differ in size. Further-
 227 more we demonstrated that extending the theory according to Staverman–
 228 Guggenheim is not necessary for the mixtures. The molar volume values
 229 employed have a significant influence on the resulting entropy of mixing and

230 therefore on the estimated ideal/reference melting point depression. Both ef-
231 fects result in a significantly different enthalpy of mixing and will thus affect
232 similarly the interaction parameter χ which we have proposed to use to quan-
233 tify the non-ideality of DESs and to describe their liquid window. Thus, for a
234 thorough characterization of the behavior of deep eutectic solutions a proper
235 choice of entropy expression and value of molar volume is a prerequisite.

236 4. Experimental

237 The experimental data reported here was directly taken from our previous
238 publications [31, 32]. The melting points of the different ratios of the mix-
239 tures were measured using melting point capillaries. The DES compositions
240 used were prepared inside a glove-box with dry nitrogen atmosphere, yielding
241 DES mixtures with moisture levels below 10 ppm. The temperature of the
242 first liquid visible at a heating rate of $5 \text{ K}\cdot\text{min}^{-1}$ was taken for the solidus
243 line (eutectic temperature); the temperature at which the last solids were
244 observed to disappear at a heating of $1 \text{ K}\cdot\text{min}^{-1}$ was taken for the liquidus
245 line (melting point).

246 The van der Waals volumes V_m and surface areas A_m have been obtained
247 following Bondi based on measured molar volumes, according to Vera *et al.*
248 [44]:

$$249 \quad V_m^{\text{Bondi}} = 0.554V_m^{\text{measured}}, \quad (17a)$$

$$250 \quad A_m^{\text{Bondi}} = 1.323 \times 10^8 \text{ cm}^{-1}V_m^{\text{Bondi}} + 6.259 \times 10^8 \text{ cm}^2 \text{ mol}^{-1}. \quad (17b)$$

251 Additionally, we estimated the van der Waals volumes and surface areas using
252 Molecular Modeling Pro, ChemSW Inc. (Fairfield, California).

253 5. Acknowledgements

254 GdW and RT acknowledge Gerard Krooshof (DSM) for useful discus-
255 sions on the thermodynamics of mixtures. The authors would like to thank
256 Marco Hendrix for the experimental support provided, and the members of
257 the ISPT “Deep Eutectic Solvents in the pulp and paper industry” consor-
258 tium for their financial and in kind contribution. This cluster consists of the
259 following organisations: Altri–Celbi, Buckman, Crown Van Gelder, CTP, DS
260 Smith Paper, ESKA, Essity, Holmen, ISPT, Mayr–Melnhof Eerbeek, Metsä
261 Fibre, Mid Sweden University, Mondi, Omya, Parenco BV, The Navigator

262 Company, Sappi, Essity, Smurfit Kappa, Stora Enso, Eindhoven University
263 of Technology, University of Aveiro, University of Twente, UPM, Valmet
264 Technologies Oy, Voith Paper, VTT Technical Research Centre of Finland
265 Ltd, WEPA and Zellstoff Pöls. Furthermore, this project received fund-
266 ing from the Bio-Based Industries Joint Undertaking under the European
267 Union’s Horizon 2020 research and innovation programme under grant agree-
268 ment Provides no. 668970. MV acknowledges the Netherlands Organisation
269 for Scientific Research (NWO) for a Veni grant (no. 722.017.005).

- 270 [1] F. Guthrie, On Eutexia, *Phys. Soc.* (1884) 462–482.
- 271 [2] F. Guthrie, On salt-solutions and attached water, *Philos. Mag. Ser. 5*
272 18 (1884) 105–120.
- 273 [3] A. P. Abbott, G. Capper, D. L. Davies, R. K. Rasheed, V. Tambyra-
274 jah, Novel solvent properties of choline chloride/urea mixtures, *Chem.*
275 *Commun.* (2003) 70–71.
- 276 [4] D. J. G. P. van Osch, L. J. B. M. Kollau, A. van den Bruinhorst,
277 S. Asikainen, M. A. Rocha, M. C. Kroon, Ionic liquids and deep eu-
278 tectic solvents for lignocellulosic biomass fractionation, *Phys. Chem.*
279 *Chem. Phys.* 19 (2017) 2636–2665.
- 280 [5] M. Zdanowicz, K. Wilpiszewska, T. Spychaj, Deep eutectic solvents for
281 polysaccharides processing. A review, *Carbohydr. Polym.* 200 (2018)
282 361–380.
- 283 [6] A. Škulcová, L. Kamenská, F. Kalman, A. Ház, M. Jablonský, K. Čížová,
284 I. Šurina, Deep eutectic solvents as medium for pretreatment of biomass,
285 *Key Eng. Mater.* 688 (2016) 17–24.
- 286 [7] K. D. O. Vigier, G. Chatel, F. Jérôme, Contribution of deep eutectic
287 solvents for biomass processing: Opportunities, challenges, and limita-
288 tions, *ChemSusChem* 7 (2015) 1250–1260.
- 289 [8] Y. Zhang, X. Ji, X. Lu, Choline-based deep eutectic solvents for CO₂
290 separation: Review and thermodynamic analysis, *Renew. Sustain. En-
291 ergy Rev.* 97 (2018) 436–455.

- 292 [9] G. García, M. Atilhan, S. Aparicio, A theoretical study on mitigation
293 of CO₂ through advanced deep eutectic solvents, *Int. J. Greenh. Gas*
294 *Control* 39 (2015) 62–73.
- 295 [10] D. Carriazo, M. C. Serrano, M. C. Gutiérrez, M. L. Ferrer, F. del Monte,
296 Deep-eutectic solvents playing multiple roles in the synthesis of polymers
297 and related materials, *Chem. Soc. Rev.* 41 (2012) 4996.
- 298 [11] B. Y. Zhao, P. Xu, F. X. Yang, H. Wu, M. H. Zong, W. Y. Lou, Biocom-
299 compatible deep eutectic solvents based on choline chloride: characterization
300 and application to the extraction of rutin from *Sophora japonica*, *ACS*
301 *Sustain. Chem. Eng.* 3 (2015) 2746–2755.
- 302 [12] Q. Zhang, K. De Oliveira Vigier, S. Royer, F. Jérôme, Deep eutectic
303 solvents: syntheses, properties and applications, *Chem. Soc. Rev.* 41
304 (2012) 7108.
- 305 [13] E. L. Smith, A. P. Abbott, K. S. Ryder, Deep eutectic solvents (DESs)
306 and their applications, *Chem. Rev.* 114 (2014) 11060–11082.
- 307 [14] A. Pelczarska, D. Ramjugernath, J. Rarey, U. Domańska, Prediction of
308 the solubility of selected pharmaceuticals in water and alcohols with a
309 group contribution method, *J. Chem. Thermodyn.* 62 (2013) 118–129.
- 310 [15] A. Diedrichs, J. Gmehling, Solubility calculation of active pharmaceu-
311 tical ingredients in alkanes, alcohols, water and their mixtures using
312 various activity coefficient models, *Ind. Eng. Chem. Res.* 50 (2011)
313 1757–1769.
- 314 [16] H. Suzuki, H. Sunada, Comparision of nicotinamide, ethylurea, and
315 polyethylene glycole as carriers for nifedipine solid dispersion systems,
316 *Chem. Pharm. Bull.* 45 (1997) 1688–1693.
- 317 [17] I. Pasquali, R. Bettini, F. Giordano, Thermal behaviour of diclofenac,
318 diclofenac sodium and sodium bicarbonate compositions, *J. Therm.*
319 *Anal. Calorim.* 90 (2007) 903–907.
- 320 [18] C. Herman, B. Haut, L. Aerts, T. Leyssens, Solid-liquid phase diagrams
321 for the determination of the solid state nature of both polymorphs of
322 (RS)-2-(2-oxo-pyrrolidin-1-yl)-butyramide, *Int. J. Pharm.* 437 (2012)
323 156–161.

- 324 [19] P. Mekala, V. Kamisetty, W. M. Chien, R. Shi, D. Chandra,
325 J. Sangwai, A. Talekar, A. Mishra, Thermodynamic modeling
326 of binary phase diagram of 2-amino-2-methyl-1, 3-propanediol and
327 TRIS(hydroxymethyl)aminomethane system with experimental verifi-
328 cation, *Calphad Comput. Coupling Phase Diagrams Thermochem.* 50
329 (2015) 126–133.
- 330 [20] K. Pielichowski, K. Flejtuch, Differential scanning calorimetry study of
331 blends of poly (ethylene glycol) with selected fatty acids, *Macromol.*
332 *Mater. Eng.* 288 (2003) 259–264.
- 333 [21] E. Palomo Del Barrio, R. Cadoret, J. Daranlot, F. Achchaq, New sugar
334 alcohols mixtures for long-term thermal energy storage applications at
335 temperatures between 70 °C and 100 °C, *Sol. Energy Mater. Sol. Cells*
336 155 (2016) 454–468.
- 337 [22] H. Schmit, C. Rathgeber, P. Hennemann, S. Hiebler, Three-step method
338 to determine the eutectic composition of binary and ternary mixtures:
339 Tested on two novel eutectic phase change materials based on salt hy-
340 drates, *J. Therm. Anal. Calorim.* 117 (2014) 595–602.
- 341 [23] B. He, V. Martin, F. Setterwall, Liquid-solid phase equilibrium study of
342 tetradecane and hexadecane binary mixtures as phase change materials
343 (PCMs) for comfort cooling storage, *Fluid Phase Equilib.* 212 (2003)
344 97–109.
- 345 [24] D. Wei, S. Han, B. Wang, Solid-liquid phase equilibrium study of binary
346 mixtures of n-octadecane with capric, and lauric acid as phase change
347 materials (PCMs), *Fluid Phase Equilib.* 373 (2014) 84–88.
- 348 [25] P. Zhao, Q. Yue, H. He, B. Gao, Y. Wang, Q. Li, Study on phase
349 diagram of fatty acids mixtures to determine eutectic temperatures and
350 the corresponding mixing proportions, *Appl. Energy* 115 (2014) 483–
351 490.
- 352 [26] G. Diarce, L. Quant, Á. Campos-Celador, J. Sala, A. García-Romero,
353 Determination of the Phase Diagram and Main Thermophysical Prop-
354 erties of the Erythritol–Urea Eutectic Mixture for its Use as a Phase
355 Change Material, *Sol. Energy Mater. Sol. Cells* 157 (2016) 894–906.

- 356 [27] A. E. Hoyt, S. J. Huang, Binary mixtures of liquid crystalline ester
357 bismaleimides, *J. Macromol. Sci. Part A* 32 (1995) 1931–1945.
- 358 [28] G. W. Smith, The influence of a metastable solid phase on eutectic
359 formation of a binary nematic liquid crystal, *Mol. Cryst. Liq. Cryst.* 30
360 (1975) 101–107.
- 361 [29] R. I. Nessim, Applicability of the Schröder-van Laar relation to multi-
362 mixtures of liquid crystals of the phenyl benzoate type, *Thermochim.*
363 *Acta* 343 (2000) 1–6.
- 364 [30] M. Sato, T. Nakano, K. I. Mukaida, Side-chain liquid crystalline homo-
365 and copolymethacrylates with a carbonate linkage between the benzyli-
366 deneaniline mesogen and ethylene chain, *Liq. Cryst.* 18 (1995) 645–649.
- 367 [31] L. J. Kollau, M. Vis, A. van den Bruinhorst, A. C. C. Esteves, R. Tuinier,
368 Quantification of the liquid window of Deep Eutectic Solvents, *Chem.*
369 *Commun.* 54 (2018) 13351–13354.
- 370 [32] L. J. Kollau, M. Vis, A. van den Bruinhorst, G. de With, R. Tuinier, Ac-
371 tivity modelling of the solid–liquid equilibrium of deep eutectic solvents,
372 *Pure Appl. Chem.* (2019).
- 373 [33] O. Redlich, A. T. Kister, On the thermodynamics of non-electrolyte
374 solutions and its technical applications: III. Systems with associated
375 components, *J. Chem. Phys.* 15 (1947) 849–855.
- 376 [34] O. Redlich, A. T. Kister, Thermodynamics of nonelectrolyte solutions -
377 x-y-t relations in a binary system, *Ind. Eng. Chem.* 40 (1948) 341–345.
- 378 [35] A. D. Pelton, C. W. Bale, Legendre polynomial expansions of ther-
379 modynamic properties of binary solutions, *Metall. Trans. A* 17 (1986)
380 1057–1063.
- 381 [36] C. J. Van Tyne, P. M. Novotny, S. K. Tarby, Solution thermodynamic
382 quantities represented by modified legendre polynomials, *Metall. Trans.*
383 *B* 7 (1976) 299–300.
- 384 [37] Z. Bouzina, M. R. Mahi, I. Mokbel, A. Negadi, C. Gouthaudier,
385 J. Jose, L. Negadi, Vapour-liquid equilibria, enthalpy of va-
386 porisation, and excess Gibbs energies of binary mixtures of

- 387 3,3-diamino-N-methyldipropylamine (DNM) (or N,N,N',N'',N''-
388 pentamethyldiethylenetriamine (PMDETA))+water, J. Chem.
389 Thermodyn. 128 (2019) 251–258.
- 390 [38] I. Díaz, M. Rodríguez, E. J. González, M. González-Miquel, A simple
391 and reliable procedure to accurately estimate NRTL interaction param-
392 eters from liquid-liquid equilibrium data, Chem. Eng. Sci. 193 (2019)
393 370–378.
- 394 [39] C. Du, R. Dong, B. Qiao, Z. Jin, T. Ye, Y. Zhang, M. Wang,
395 Construction and evaluation of ternary solid-liquid phase diagram of
396 pyraclostrobin (form IV) and its intermediate in ethanol and N,N-
397 dimethylformamide, J. Chem. Thermodyn. 128 (2019) 1–9.
- 398 [40] H. Renon, J. M. Prausnitz, Local compositions in thermodynamics
399 excess functions for liquids mixtures, AIChE J. 14 (1968) 116–128.
- 400 [41] G. J. Krooshof, R. Tuinier, G. de With, On the calculation of nearest
401 neighbors in activity coefficient models, Fluid Phase Equilib. 465 (2018)
402 10–23.
- 403 [42] E. A. Guggenheim, Statistical thermodynamics of co-operative systems
404 (a generalization of the quasi-chemical method)., Trans. Faraday Soc.
405 44 (1948) 1007–1012.
- 406 [43] A. J. Staverman, The Entropy of High Polymer Solutions., Recl. Trav.
407 Chim. Pays-Bas 69 (1950) 163–174.
- 408 [44] J. H. Vera, S. G. Sayegh, G. A. Ratcliff, A quasi lattice-local composition
409 model for the excess Gibbs free energy of liquid mixtures, Fluid Phase
410 Equilib. 1 (1977) 113–135.
- 411 [45] R. H. Fowler, E. A. Guggenheim, Statistical Thermodynamics, Cam-
412 bridge University Press, Cambridge, 1939.

413 **Appendix A. Additional results**

Table A.1: Results for the mixtures of erythritol, succinic acid, and pimelic acid with Pe_4NBr . Listed are the theory used for the entropy of mixing s , the interaction parameter $\chi = p_0$, the second fit parameter p_1 [32], the eutectic temperature T_e , the eutectic composition x_e , and the standard error SE between the fit of the phase diagram and the data points.

System	s	χ	p_1	T_e [K]	x_e	SE [K]
Erythritol– Pe_4NBr	s^x	−2.61	0	346.9	0.56	2.50
	s_{Bondi}^ϕ	−1.68	−0.88	346.4	0.59	1.99
	s_{Bondi}^θ	−1.71	−0.87	346.4	0.59	1.99
	s_{MMP}^ϕ	−1.88	−0.75	346.4	0.59	2.00
	s_{MMP}^θ	−1.90	−0.74	346.4	0.59	2.00
Succinic acid– Pe_4NBr	s^x	−4.86	1.01	349.9	0.65	3.39
	s_{Bondi}^ϕ	−3.93	0	348.3	0.64	3.88
	s_{Bondi}^θ	−3.96	0	348.2	0.64	3.91
	s_{MMP}^ϕ	−4.17	0	347.8	0.64	4.11
	s_{MMP}^θ	−4.18	0	347.8	0.64	4.13
Pimelic acid– Pe_4NBr	s^x	−6.40	−2.73	309.6	0.53	1.85
	s_{Bondi}^ϕ	−5.86	−2.93	309.6	0.53	1.90
	s_{Bondi}^θ	−5.87	−2.93	309.6	0.53	1.90
	s_{MMP}^ϕ	−5.95	−2.88	309.6	0.53	1.88
	s_{MMP}^θ	−5.95	−2.88	309.6	0.53	1.88

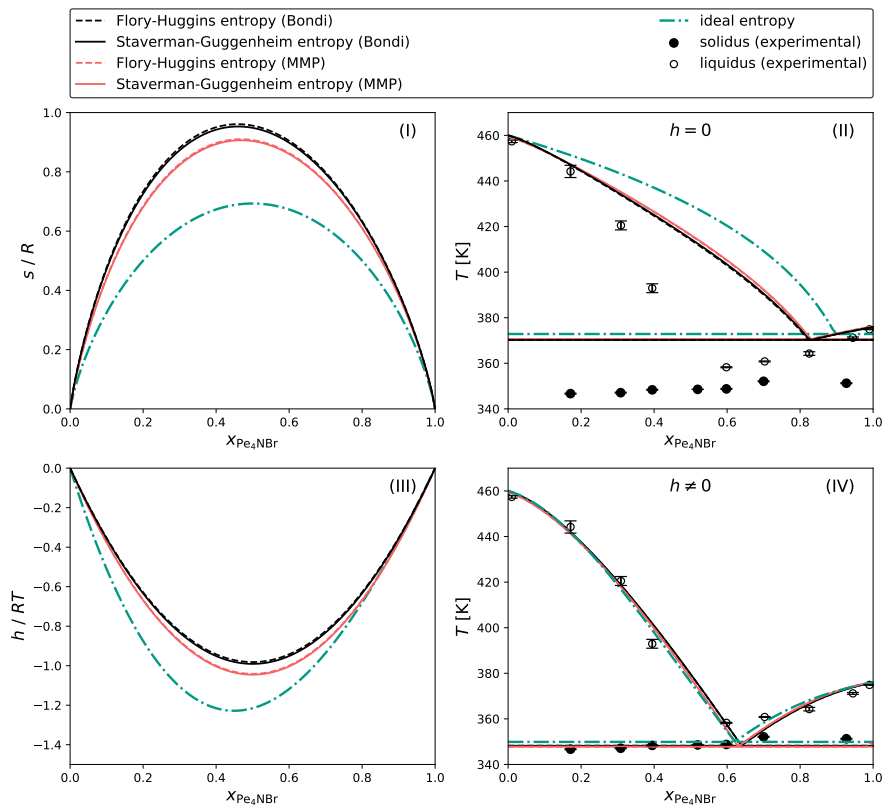


Figure A.1: Diagrams for Pe_4NBr –succinic acid describing (I) the entropy of mixing, (II) the melting point depression predicted based on entropy alone ($h = 0$, curves) compared to experimental data (symbols), (III) the enthalpy of mixing obtained after fitting measured melting point depressions, and (IV) the fitted melting point depressions compared to experimental data. Various entropy models are used: ideal, Flory–Huggins, and Staverman–Guggenheim. The latter two are combined with van der Waals volumes and areas estimated using the Molecular Modeling Pro software (MMP) and Bondi’s method. Experimental data taken from Ref. 32.

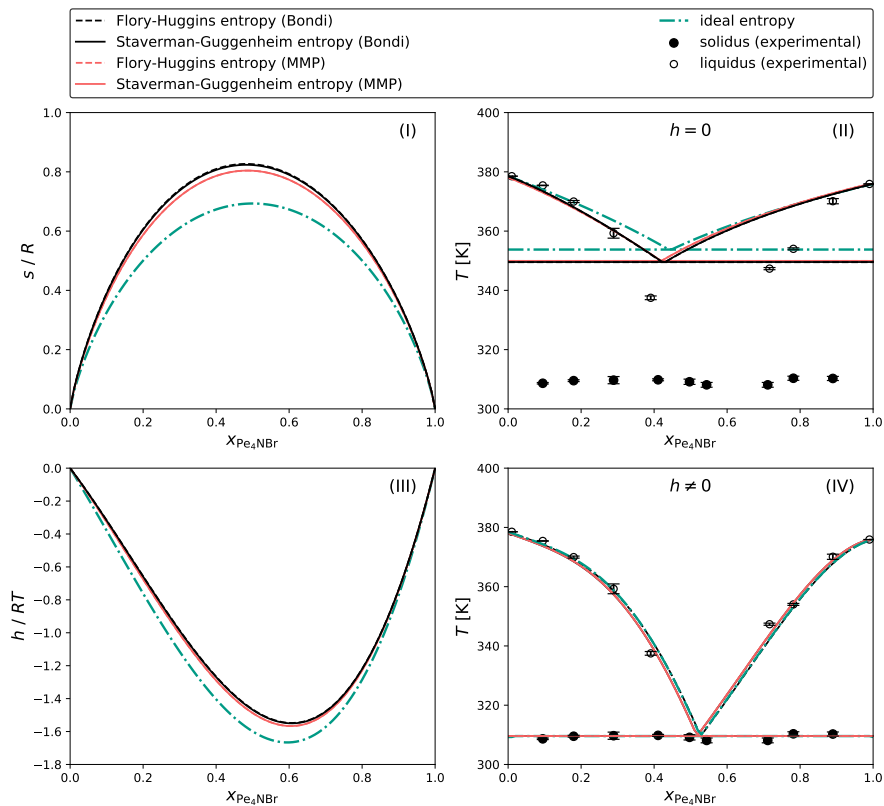


Figure A.2: Diagrams for Pe_4NBr –pimelic acid describing (I) the entropy of mixing, (II) the melting point depression predicted based on entropy alone ($h = 0$, curves) compared to experimental data (symbols), (III) the enthalpy of mixing obtained after fitting measured melting point depressions, and (IV) the fitted melting point depressions compared to experimental data. Various entropy models are used: ideal, Flory–Huggins, and Staverman–Guggenheim. The latter two are combined with van der Waals volumes and areas estimated using the Molecular Modeling Pro software (MMP) and Bondi’s method. Experimental data taken from Ref. 32.